Keck Spectroscopy of Objects with Lens-like Morphologies in the Hubble Deep Field[1,2]

Stephen E. Zepf[3], Leonidas A. Moustakas, and Marc Davis
Department of Astronomy, University of California, Berkeley, CA 94720
e-mail: szepf, lmoustakas, mdavis@astro.berkeley.edu

ABSTRACT

We present spectroscopy from the Keck telescope of three sets of objects in the Hubble Deep Field which have lens-like morphologies. In the case of J123641+621204, which is composed of four objects with similar colors and a mean separation of $\lesssim 0\farcs8$, we find at least two distinct components at redshifts of $z = 3.209$ and $z = 3.220$ which are separated by $0\farcs5$ spatially. Each of these components has narrow Lyα emission, and possibly NV emission and SiIV and CIV in absorption or with a P-Cygni profile. The second case is J123652+621227, which has an arc-like feature offset by $1\farcs8$ to the southwest of a red elliptical-like galaxy, and a "counterimage" offset $1\farcs4$ on the opposite side. We tentatively find a single line at 5301Å at the spatial position of the counterimage, and *no* corresponding emission line at the position of the arc. The colors of the counterimage are consistent with the identification of this line as Lyα at $z = 3.36$. The colors of the arc are different than those of the counterimage, and thus both the colors and spectra indicate that this object is unlikely to be a gravitational lens. For a third lensing candidate (J123656+621221), which is a blue arc offset by $0\farcs9$ from a red, elliptical-like galaxy, our spectroscopy does not clearly resolve the system spatially, complicating the interpretation of the spectrum. We discuss possible identifications of a number of absorption features and a very tentative detection of a pair of emission lines at 5650Å and 5664Å, and find that gravitational lensing remains a possibility in this case. We conclude that the frequency of strong gravitational lensing by galaxies in the HDF appears to be very low. This result is difficult to reconcile with the introduction of a cosmological constant to account for the large number of faint blue galaxies via a large volume element at high redshift, and tends to favor models in which very faint galaxies are at fairly modest redshifts.

---

[1]Based on observations obtained at the W.M. Keck Observatory, which is operated jointly by the California Institute of Technology and the University of California

[2]Based on observations with the NASA/ESA Hubble Space Telescope, obtained at the Space Telescope Science Institute, which is operated by AURA, Inc., under NASA contract NAS 5-26555

[3]Hubble Fellow

Subject headings: cosmology: gravitational lensing - cosmology: observations - galaxies: distances and redshifts - galaxies: evolution - galaxies: individual

1. Introduction

Gravitational lensing by galaxies is of interest both because it provides constraints on the mass distribution of the lensing galaxy, and because it allows the study of galaxies at higher redshifts than would otherwise be possible because of the magnification of the lensed object. The Hubble Space Telescope (HST) has proven to be very useful for gravitational lensing studies because of its ability to obtain high resolution images of faint objects. This utility has been demonstrated both by studies of previously identified lensing candidates (e.g. FSC 10214+4724, Eisenhardt et al. 1996), and the discovery of new candidate lenses (e.g. Ratnatunga et al. 1995).

The HST images of the Hubble Deep Field (HDF) provide a rich ground for gravitational lens searches because of the combination of deep exposures in multiple colors and the high spatial resolution of the HST (Williams et al. 1996). A visual inspection of the field reveals several possible candidate lensing systems (e.g. Hogg et al. 1996). These include a configuration of four compact galaxies with similar blue colors, separated by $\lesssim 1\farcs0$ (J123641+621204, or in our notation L4.1), a red "elliptical" with a blue "arc" offset by about $1\farcs8$ to the southwest and a potential counterimage on the other side (J123652+621227, or L3.1), and a red "elliptical" with a blue "arc" offset by about $0\farcs9$ to the south (J123656+621221, or L3.2).

Spectroscopy of the constituent objects is critical for determining the nature of these candidate gravitational lens systems. Therefore, as part of a modest program of spectroscopy of galaxies in the HDF, we used the Keck telescope to obtain low-resolution spectra of objects in these candidate lenses with the aim of determining their redshifts and spectral characteristics. The observations themselves are described in § 2, the results of the analysis of the data in § 3, and the implications of these results are discussed in § 4.

2. Observations

Spectra of objects in the HDF were obtained on 1996 March 15 (UT) with the Keck 10-m telescope and the Low-Resolution Imaging Spectrograph (LRIS, Oke et al. 1995). The LRIS slit-mask facility allowed us to obtain spectra of many objects simultaneously. We designed two slitmasks, each of which contained about 20 objects in the HDF itself and its flanking fields. The slitlets were $0\farcs7$ wide. The spectra were obtained using the 300 l/mm grating, which provided wavelength coverage from about 5000Å through 9500Å with the exact coverage dependent on the location of the slitlet, and with declining sensitivity at the red end of this range. With the 24μm pixels of the Tektronix CCD, the wavelength scale is approximately 2.4Å/pixel and the spatial scale is $0\farcs214$/pixel.

In selecting our objects, we specifically targeted the three sets of objects in the HDF which we found to be the most likely lensed systems. True-color images of these sets of objects and the orientation of our slit positions is shown in Figure 1 (Plate 1). The positions, magnitudes, and

colors of the objects in these candidate lens systems are given in Table 1. The position angles of the two masks were chosen so that the slitlets passed through both the candidate lens and lensed object for the two systems in which both are identifiable. This corresponds to a position angle of 19° (PA19) for L3.2 and 61° (PA61) for L3.1. A slitlet was placed across the system of four similar objects (L4.1) at both position angles.

Our observations consist of 80 minutes of integration time with the PA61 mask and 60 minutes for the PA19 mask, each of which was divided into two exposures. From images taken during the alignment procedure, we estimate the seeing was about $0\farcs9$. The reduction of these data is described in detail in Moustakas et al. (1996). Briefly, after standard CCD reduction techniques, the two exposures were combined using bad pixel maps to eliminate cosmic rays. The combined image was checked by eye for the few cosmic rays which escaped detection in the first pass. The combined image was then transformed to linear wavelength scale using arc lamps observed after each exposure.

One-dimensional spectra were then extracted from the two-dimensional data. The location on the slitlet of each extraction was based on the observed location of flux. In all cases, this corresponds to the expected location of a target object. The one-dimensional spectrum was smoothed with a gaussian of $\sigma = 3.0$Å, which is the approximate instrumental resolution. No further smoothing was performed. A relative flux calibration of the spectra was made using a spectrophotometric standard observed with LRIS in long-slit mode on an earlier observing run with a very similar setup (kindly provided by H. Spinrad and D. Stern). Although this is clearly far from ideal for flux calibration, the result is consistent with a previously obtained spectrum of one of our targets. The resulting one-dimensional spectra are described in detail in the following section.

3. Analysis

3.1. L4.1 (J123641+621204)

The extracted spectra of this set of objects are shown in Figure 2, along with a spectrum obtained for the same objects with a wider slit by Steidel et al. (1996, hereafter SGDA). This figure indicates that our spectra confirm SGDA's general identification of Lyα emission at $z \simeq 3.22$, and possibly their identification of SiIV absorption at the same redshift. This redshift is consistent with the colors of the objects given in Table 1, as the redshifted Lyman break provides a natural explanation for the very red F300W − F450W color. In fact, the objects were selected by SGDA to be candidate $z \sim 3$ galaxies on the basis of their colors.

A closer look at our spectra shows that at both of our position angles, the emission lines have two distinct components. Based on Lyα, the redshifts of these components are $z = 3.220$ and $z = 3.209$, corresponding to a rest frame velocity difference of 800 $\mathrm{km\,s^{-1}}$. Moreover, our

two-dimensional spectra indicate that the different velocity components are at different spatial locations. This is shown in Figure 3 (Plate 2), in which the Lyα lines are at the same location or only slightly offset along the slit for PA61, but are separated by several pixels for PA19. A correlation between velocity and position had been tentatively suggested by SGDA. *The detection of a different spatial location for the different velocity components rules out gravitational lensing as the cause of this compact configuration of high redshift objects.*

With our two position angles, we can attempt to identify which of the four objects is responsible for each feature. Because the emission lines are at roughly the same position on the PA61 slitlet, the likely candidates are the northern and southern objects, as these are the only two at roughly the same position along the slit at this angle. This tentative identification appears to be confirmed by the offset observed on the PA19 slitlet, which is exactly that expected if the two emission components are from these two objects. However, as a caution we note the seeing was only marginal for resolving this system, and a firm identification of individual spatial components with velocity components awaits spectral data with better spatial information.

We also note that both redshift components appear to have NV emission which is strong relative to Lyα, and which is redshifted compared to its expected location given the z determined from Lyα. Strong NV emission is also present in SGDA's spectrum, as is the offset of the peak emission to slightly higher redshift than that of the corresponding Lyα feature. The relative strength of the high ionization NV line is suggestive of an AGN (e.g. Kinney et al. 1993). However, the redward peak of the NV feature and the possible evidence for some P-Cygni absorption blueward of the expected line center suggest that there may also be a massive star component to the NV emission. Therefore, this system appears to be composed of two or more star-forming galaxies, possibly with AGN, separated by roughly 10 kpc and 800 $\mathrm{km\,s^{-1}}$.

3.2. L3.1 (J123652+621227)

From west to east, our slitlet for this system crossed the "arc", the central "elliptical" and then the "counterimage" (see Figure 1). An emission line at 5301Å at the position of the counterimage is the only emission feature detected along this slitlet. A one-dimensional spectrum extracted at the position of the counterimage is shown in Figure 4. The two-dimensional spectrum in the wavelength region around the detected emission line is shown in Figure 3 (Plate 2). The emission feature is visible on each separate exposure. A faint red continuum at the position of the elliptical can be seen on the two-dimensional spectrum, but the signal is insufficient for any analysis. An even weaker blue continuum is visible on the two-dimensional image at the position of the arc. Most importantly, no emission line is seen in the arc spectrum in the range from 5000Å to 7200Å.

The presence of an emission line at the position of the counterimage and the absence of any corresponding line at the position of the arc is evidence against a lensing origin for this system.

However, the emission feature is not overwhelmingly strong, so it is interesting to consider other data. The colors of the objects given in Table 1 provide independent evidence that the arc feature and counterimage are not lensed images of a single object. Specifically, the counterimage has a significantly bluer F450W−F606W color than the arc. Although slightly different colors are possible for different arc features (Hogg et al. 1996), the combination of the colors and our spectral data favor the more straightforward interpretation that the arc and counterimage are different galaxies.

The colors can also help in the identification of the single emission line of the counterimage. The colors show that the counterimage has a flat spectrum from F814W through F450W, and then probably reddens into the F300W bandpass. The flat spectral shape is characteristic of the star-forming galaxies, and the red F300W−F450W color, if real, suggests that $z \gtrsim 2.5$, as a result of the Lyman break redshifting through the F300W bandpass (e.g. SDGA). Unfortunately, the faintness of the counterimage means that the absence of a detection only requires F300W−F450W > 0.19 at the 3σ level, and F300W−F450W > 1.39 at the 1σ level. The colors do not clearly establish the presence or absence of a Lyman break. However, it is difficult to find examples of lower redshift galaxies with flat spectra from F814W through F450W and a significantly redder F300W−F450W color.

Guided by the colors, a natural identification for the single strong emission line is Lyα. This identification places the object at $z = 3.36$. We find no other emission lines in the spectrum, which may be taken as support for this identification, since we might expect to see [OIII] 4959, 5007 and Hβ lines if the observed line at 5301Å is identified as [OII] 3727 . If the Lyα identification is correct, then the red magnitude of $AB_{606+814} = 27.2$ corresponds to a rest frame luminosity of about $L_{1600} = 4.8 \times 10^{39}$ ergs s^{-1}Å^{-1} for $q_0 = 0.5$, and 1.5×10^{40} ergs s^{-1}Å^{-1} for $q_0 = 0.05$, with $H_0 = 75$ km s^{-1}Mpc^{-1} in both cases. For comparison, a star formation rate of 1 $M_\odot$yr^{-1} with a Salpeter IMF gives produces roughly $L_{1600} = 10^{40}$ ergs s^{-1}Å^{-1} (e.g. Leitherer, Robert, & Heckman 1995).

3.3. L3.2 (J123656+6212210)

The extracted spectrum of this pair of objects is shown in Figure 5. Because the separation between the red "elliptical" and the blue "arc" is only about $0''.9$, the objects are not clearly spatially resolved in our two-dimensional spectrum. Therefore, the extracted spectrum plotted in Figure 5 is a composite of both objects. The composite nature of this spectrum complicates the identification of the lines and the determination of the redshift of the objects.

In the one-dimensional spectrum, we tentatively identify a number of absorption features and a pair of emission lines at 5650Å and 5664Å. It is natural to associate the absorption features and most of the continuum with the elliptical, because of its red colors and brighter magnitude over the range of wavelengths covered by our spectrum. Similarly, it is natural to identify the

possible emission lines with the arc, which has blue colors indicative of a nearly flat spectrum ($f_\nu \propto \nu^0$) across the range of bandpasses. The continuation of the flat spectrum through the F300W bandpass also puts an upper limit of about 2.5 on the redshift of the arc, because of the absence of a Lyman break. Moreover, the absence of any strong single emission line in such a blue spectrum (indicative of a starburst or nuclear activity), suggests that the redshift is greater than about one, or we would expect to see lines from either [OII] or [OIII] and Hβ. Thus, the combination of the colors and the spectrum suggests that the arc is at $1.0 \lesssim z \lesssim 2.5$. Given this range, our most probable identification of the pair of emission lines is the MgII doublet at 2798Å, which would place the arc at a redshift of 1.02. This redshift is clearly very tentative.

Adopting a similar approach of first constraining the range of reasonable redshifts from the colors, we find that the elliptical galaxy has colors which are consistent with those of an elliptical at a redshift of roughly 0.8. This redshift estimate may not be unique, as it might also be possible to fit the colors with a redshift around 3.5. However, in the high redshift case, the object is much brighter than an ordinary galaxy, while at $z = 0.8$, the luminosity of the object is close to L_*. Detailed photometric redshift analyses by other groups also favor the lower redshift, with Cowie (1996) finding $z \simeq 1.1$ and the approach of Lanzetta, Yahil, & Fernández-Soto (1996) giving $z \simeq 0.72$ (Yahil 1996). At either redshift, we have failed to convincingly match the observed absorption lines with prominent stellar and interstellar absorption lines. For the reasons given above, a lower redshift appears to be favored, but this hypothesis remains unproven by our spectroscopy. Therefore, lensing remains a viable possibility in this case, with our favored redshift being slightly greater than one for the arc and somewhat less than one for the elliptical. However, further spectroscopy is required to confirm or reject this hypothesis.

4. Discussion

Our primary result is that gravitational lensing is unlikely to be the cause of the configuration of two of the three candidate lensing systems we have studied. Specifically, we find that the system L4.1 has two distinct velocity components at slightly different positions. We have also found some evidence against gravitational lensing in the L3.1 system, which was identified by Hogg et al. (1996) as the most probable candidate for lensing in the HDF. In the case of the L3.2 system our data are consistent with lensing, but are inconclusive. It is therefore plausible that there is no more than one multiply imaging lensing system among the approximately 750 objects in the HDF to a limiting magnitude of roughly F814W$_{AB} < 27$ for the observed magnitudes of the sources. Although we have not obtained spectra for every object in the HDF, we targeted the three systems which appeared to us to be the most likely lensing cases, and two of these three have been similarly identified by other groups (e.g. Hogg et al. 1996). Therefore, we consider it unlikely that there is a large population of undiscovered multiple lensing systems within the magnitude limit given above.

We can estimate the observed frequency of lensing by combining the number of lenses

determined above with the number of potential sources in the HDF. As a starting point we adopt the number of objects with F814W$_{AB}$ < 27, which is similar to the magnitude of the fainter candidates we studied. This limit gives roughly 750 objects which are potential lens sources. The true number of potential sources is likely to be greater, since this number does not account for magnification of fainter galaxies. Taking our observational limit of one lensing system, we derive a rough lensing rate of around 0.000-0.002; this estimate clearly has large uncertainties due to the small numbers involved.

Even with the large uncertainties, it is difficult to reconcile these observations with the high lensing rates expected in some cosmological models. In particular, cosmological models with large Λ in which the large numbers of faint blue galaxies are a normal evolving galaxy population appear to be inconsistent with the low rate of multiply imaging lensing of very faint galaxies. Although a detailed model of lensing of galaxies in the HDF is not yet available, it is notable that the frequency of multiply imaging lensing derived above is about an order of magnitude lower than that observed for quasars, which itself places tight constraints on the cosmological constant (e.g. Kochanek 1996 and references therein). Therefore, a high Λ, passive evolution model for faint galaxies is only viable if there is some combination of effects which reduce the observed frequency of galaxy lensing by more than an order of magnitude compared to quasars. A factor of several difference is expected from the lower magnification bias likely for galaxies relative to quasars. However, the faint galaxies are observed to be compact and are expected in these models to be at rather high redshift, both of which make it hard to reduce the observed lensing rate relative to quasars by more than an order of magnitude. With better statistics, it may be possible to constrain other models for the faint blue galaxies. For example, if the lensing rate for the faint blue galaxies can be shown to be less than that for quasars and radio sources, the simplest explanation would be that the faint blue galaxies are at modest redshifts compared to these other source populations.

This work is based in part on observations obtained at the W.M. Keck Observatory, which is operated jointly by the California Institute of Technology and the University of California, and would not have been possible without the Keck telescope and the staff who operate it. We also acknowledge Bob Williams and the HDF team for carrying out the survey and making the data immediately available. We thank Chuck Steidel for providing his spectrum of J123641+621204 in advance of publication, and Drew Phillips for providing his software for mask design and alignment, both of which were very useful. Aaron Barth, Joe Silk, and Hy Spinrad, provided useful comments during the progress of this work, and Len Cowie and Amos Yahil provided photometric redshifts in advance of publication. The suggestions of an anonymous referee improved the final paper. This research is supported by NSF grant AST92-21540. S.E.Z. acknowledges support from NASA through grant number HF-1055.01-93A awarded by the Space Telescope Science Institute, which is operated by the Association of Universities for Research in Astronomy, Inc., for NASA under contract NAS5-26555.

REFERENCES

Cowie, L.L. 1996, private communication

Eisenhardt, P.R., Armus, L., Hogg, D.W., Soifer, B.T., Neugebauer, G., & Werner, M.W. 1996, ApJ, 461, 72

Hogg, D.W., Blandford, R., Kundic, T., Fassnacht, C.D., Malhotra, S. 1996, ApJ, 467, L73

Kinney, A.L., Bohlin, R.C., Calzetti, D., Panagia, N. 1993, ApJS, 86, 5

Kochanek, C. 1996, ApJ, 466, 638

Lanzetta, K.M., Yahil, A., Fernández-Soto, A. 1996, Nature, 381, 759

Leitherer, C., Robert, C. & Heckman, T. 1995, ApJS, 99, 173

Moustakas, L.A., Zepf, S.E., & Davis, M. 1996, AJ, in preparation

Oke, J.B., et al. 1995, PASP, 107, 375

Ratnatunga, K.U., Ostrander, E.J., Griffiths, R.E., & Im, M. 1995, ApJ, 453, L5

Steidel, C.C., Giavalisco, M., Dickinson, M., & Adelberger, K.L. 1996, AJ, 112, 352 (SGDA)

Yahil, A., 1996, private communication

Williams, R.E., et al. 1996, AJ, 112, 1335

This preprint was prepared with the AAS LaTeX macros v4.0.

Table 1. Photometric Data for HDF Objects with Lens-like Morphologies

Object Name	F814W[1]	(F606W - F814W)	(F450W - F606W)	(F300W - F450W)[2]
L4.1-N	25.29	0.19	0.76	2.72 (> 2.31)
W	26.04	0.28	1.02	$\cdots$ (> 1.21)
S	26.61	0.20	0.95	$\cdots$ (> 0.79)
E	26.33	0.32	0.92	1.83 (> 0.98)
L3.2-arc	26.18	0.27	0.05	0.17
ell	23.77	1.74	1.88	0.47
L3.1-arc[3]	26.72	0.41	0.42	1.67 (> 0.99)
cnt	27.18	0.41	0.78	$\cdots$ (> 0.19)
ell	25.02	1.79	1.68	0.95 (> 0.06)

[1]AB magnitude within $0\farcs2$ radius aperture.

[2]If the counts within the $0\farcs2$ radius aperture are less than 3σ above the background fluctuations within the same aperture, the color at the 3σ limit is given in parentheses. No data indicates that the counts are below 1σ of the background.

[3]Aperture centered at the middle of the primary arc.

Figure Captions

Figure 1 - True-color images of the lens-like mophology objects, in which the blue plane is from the F450W image, the green from the F606W image, and the red from the F814W image. Each image is oriented with North up and East to the left, and is $8''.0$ on a side. The white lines indicate the position angles of the slits. The image on the top left is L3.1 (J123652+621227), on the top right is L3.2 (J123656+621221), and on the bottom is L4.1 (J123641+622104).

Figure 2 - The extracted spectra for L4.1 (J123641+622104). The two panels are our spectra at the position angles shown, and the bottom panel is the spectrum from SGDA. All of these show Lyα and NV emission, and SiIV absorption. Both the Lyα and NV emission lines are double-peaked, and the NV feature is redshifted relative to Lyα in all of the spectra. The higher resolution of our spectra relative to SGDA's spectrum results primarily from our narrower slit.

Figure 3 - The top two images are two-dimensional spectra of the L4.1 system (J123641+622104) at PA=19° and PA=61° respectively. These show a spatial shift of about $0''.5$ at PA=19° and little or no shift at PA=61°. The lower image is the two-dimensional spectrum of the L3.1 (J123652+621227) system. The images have been smoothed by an elliptical Gaussian with a FWHM of the instrumental resolution in the wavelength direction and the seeing in the spatial direction. The width of this smoothing is noted in the upper left corner of each image.

Figure 4 - The extracted spectra for system L3.1 (J123652+621227). The top panel shows the spectrum at the position of the counterimage, and the bottom panel shows the spectrum at the position of the arc-like feature. The emission line at 5301Å in the spectrum of the counter-image is not present in the spectrum at the position of the arc, suggesting that this system is not a gravitational lens.

Figure 5 - The extracted spectrum of system L3.2 (J123656+621221). The spectrum is a composite of the elliptical and the arc, as these were not clearly resolved spatially in our two-dimensional spectrum. A tentative pair of emission lines and a number of likely absorption features are marked.

This figure "Figure1.jpg" is available in "jpg" format from:

http://arXiv.org/ps/astro-ph/9606153v2

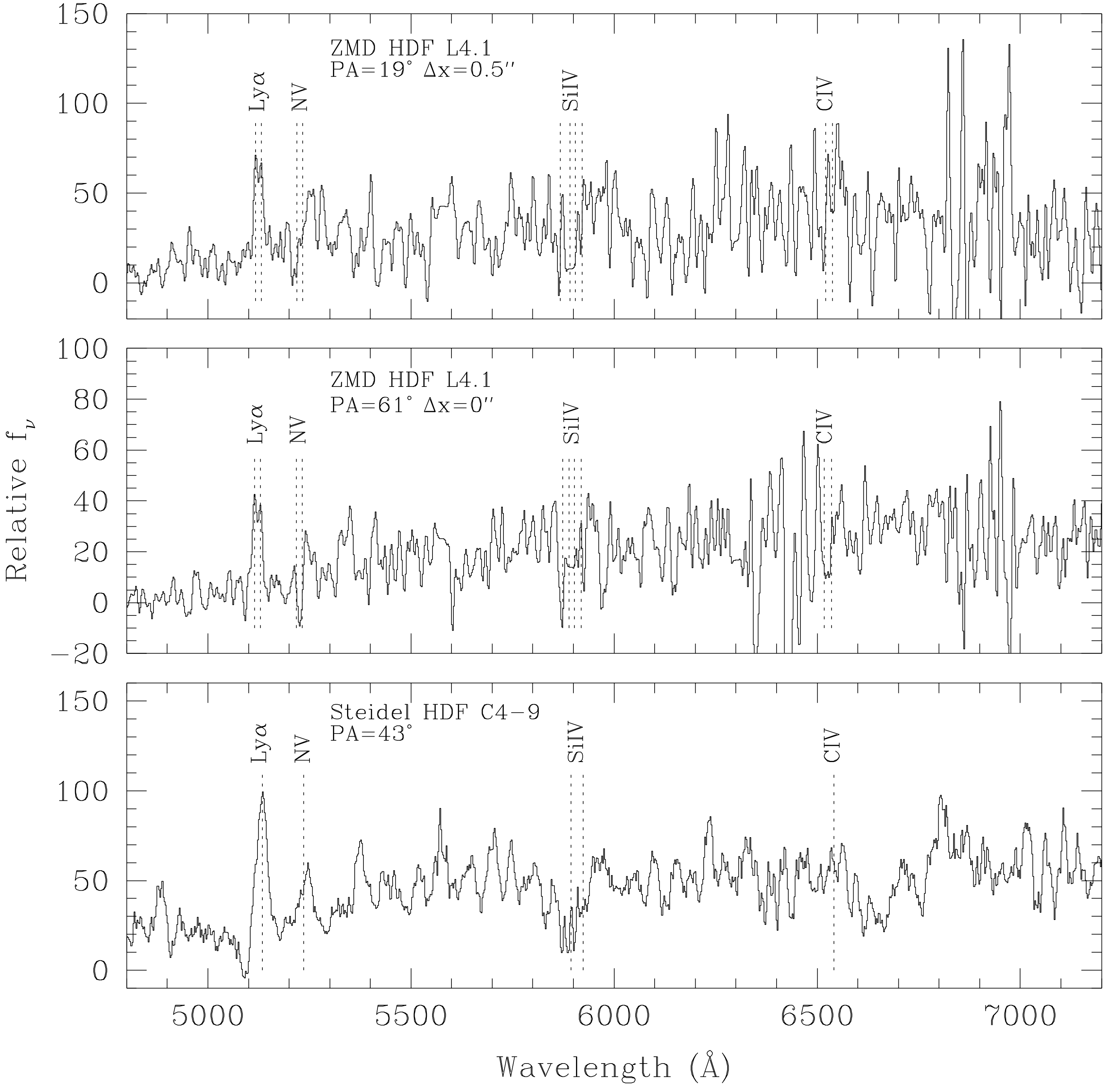

ZMD HDF L4.1
PA=19° Δx=0.5″
ZMD HDF L4.1
PA=61° Δx=0″
Steidel HDF C4-9
PA=43°
Lyα
NV
SiIV
CIV
Relative f$_\nu$
Wavelength (Å)

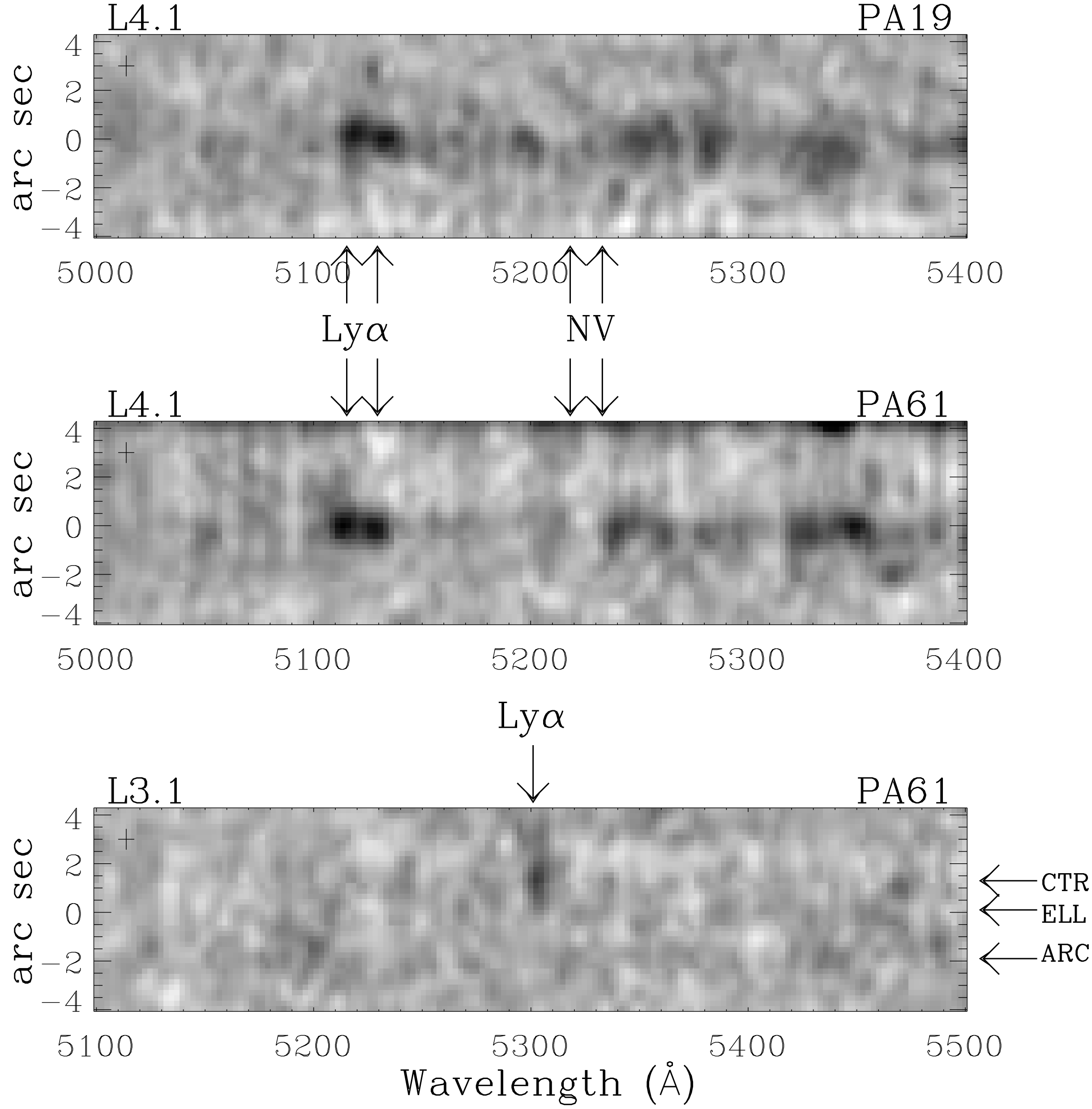

L4.1
PA19
arc sec
4
2
0
−2
−4
5000
5100
5200
5300
5400
Lyα
NV
L4.1
PA61
arc sec
L3.1
PA61
CTR
ELL
ARC
5500
Wavelength (Å)

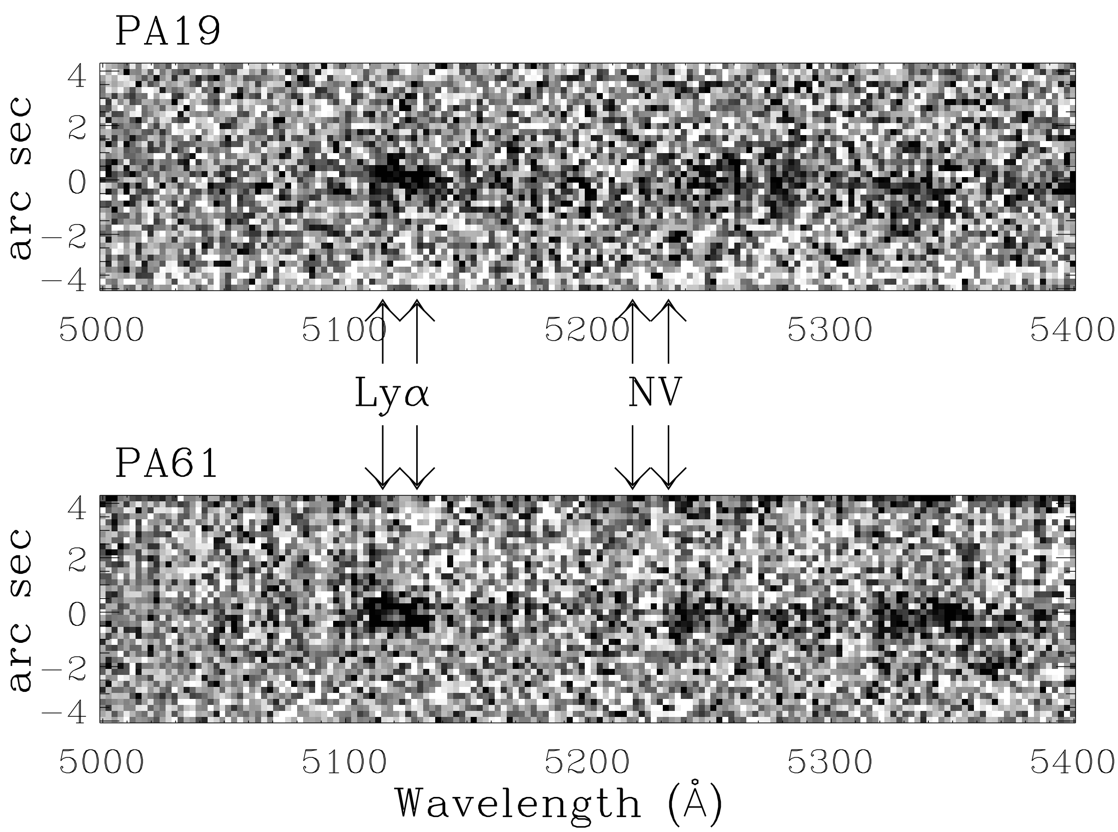
PA19
arc sec
4
2
0
−2
−4
5000
5100
5200
5300
5400
Lyα
NV
PA61
arc sec
4
2
0
−2
−4
5000
5100
5200
5300
5400
Wavelength (Å)

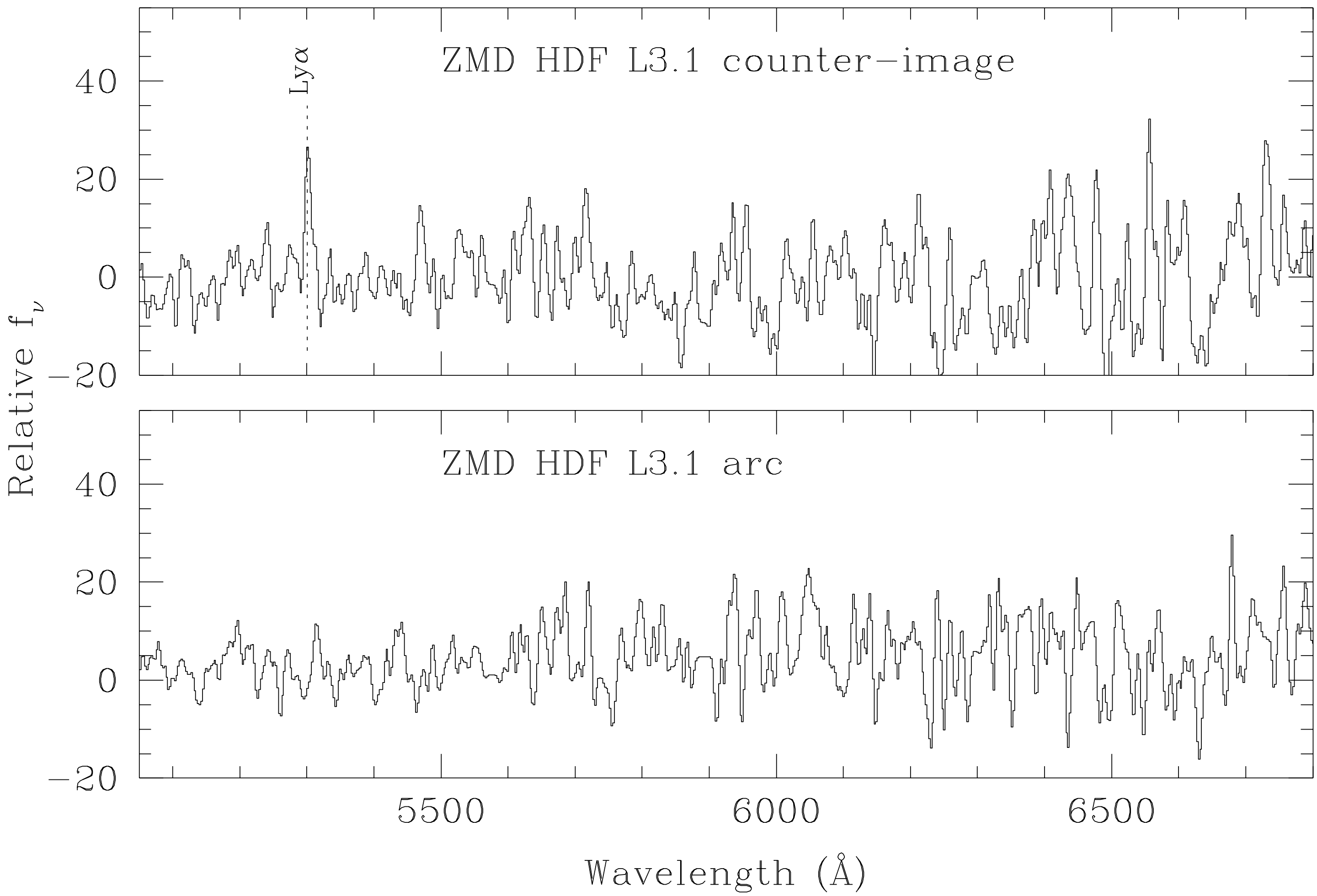

ZMD HDF L3.1 counter-image
Lyα
ZMD HDF L3.1 arc
Relative f_ν
Wavelength (Å)
40
20
0
−20
5500
6000
6500

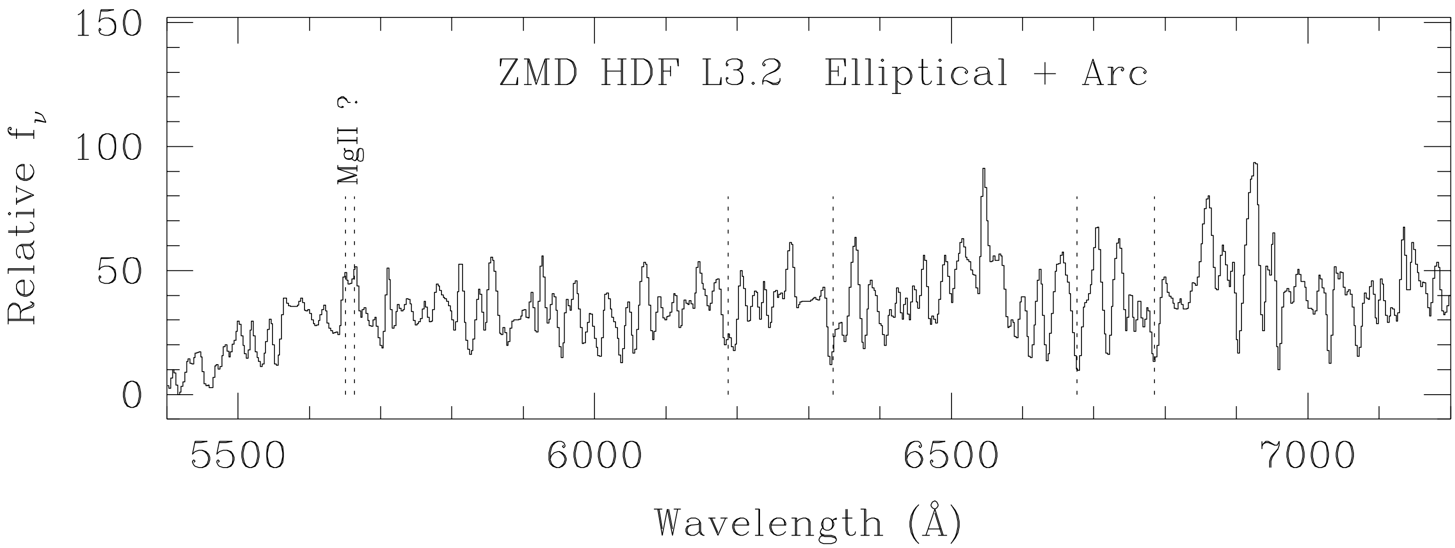

ZMD HDF L3.2 Elliptical + Arc
MgII ?
Relative f$_\nu$
150
100
50
0
5500
6000
6500
7000
Wavelength (Å)